doi:10.2533/chimia.2024.50 Chimia 78 (2024) 50–58

In situ/In vivo Optical Microspectroscopy to Probe the Emergence of Morphology

Natercia Barbosa, Oscar Urquidi, Johanna Brazard, and Takuji B. M. Adachi*

Abstract: Morphology governs function. Yet, understanding and controlling the emergence of morphology at the molecular level remains challenging. The difficulty in studying the early stage of morphology formation is due to its stochastic nature both spatially and temporally occurring at the nanoscale. This nature has been particularly detrimental for the application of optical spectroscopy. To overcome this problem, we have been developing new *in situ/in vivo* optical spectroscopy tools, which are label-free and non-invasive. This account highlights several examples of how optical spectroscopy can become an important tool in studying the birth of morphology.

Keywords: Biomineralization · Crystallization · Laser tweezer Raman microspectroscopy · Single crystal nucleation spectroscopy (SCNS) · Time-resolved dynamic light scattering microscopy (micro-DLS)

Natercia Barbosa is a PhD candidate at the University of Geneva (Takuji Adachi group). She obtained her MSc in Geneva under the supervision of Dr. Montserrat Filella and Prof. Takuji Adachi. In her masters thesis, she investigated the biomineralization of barite in freshwater algae. Currently, she is pursuing her interest on biomineralization by using *in situ* spectroscopic methods to study different systems, such as organic and carbonate biominerals.

Oscar Urquidi is a PhD candidate at the University of Geneva (Takuji Adachi group), holding an MSc in photonics from the University of Vigo and a bachelors degree in electromechanical engineering from Universidad Privada Boliviana. He is passionate about solving complex problems of interdisciplinary nature and developing new technologies.

Johanna Brazard is a senior scientist at the University of Geneva. She obtained her PhD at the ENS (France) under the supervision of Dr. Pascal Plaza. After postdoctoral trainings at the the University of Texas at Austin (Paul Barbara/David Vanden Bout group) and CEA Paris-Saclay (Francis Perrin Laboratory), she obtained a CNRS research position in France. She took sabbatical leave to work at New York University (Daniel Turner group) to gain experience in 2D electronic spectroscopy. After working at IPCMS in Strasbourg as a CNRS researcher, she is currently on sabbatical leave at the University of Geneva.

Takuji B. M. Adachi is a tenure-track assistant professor at the University of Geneva. He obtained his PhD at the University of Texas at Austin under the supervision of Prof. Paul Barbara and Prof. David Vanden Bout. After postdoctoral trainings at the University of Regensburg (John Lupton group), New York University (Michael Ward group) and the University of Strasbourg (Thomas Hermans group), he started his independent research at the Department of Physical Chemistry at the University of Geneva on September 2019.

1. Introduction

The study of structure-property relationships has been an important research activity for a wide range of materials and biological systems. On the contrary, how 'the emergence of morphology' occurs, remains an open question, even though it is critical to establish the atomic/molecular level understanding of morphological formation to rationally design materials, drugs, and prevent various unwanted pathological diseases *etc*.

Our group is interested in the early stage of morphological formation or phase transition in a wide range of systems, such as organic/inorganic crystals,[1–3] supramolecular polymers,[4,5] and biomineralization.[6–8] These wide ranges of topics share a common phenomenon: upon the change of concentration, pH, temperature, or pressure, a system may undergo a metastable phase and eventually a nucleation of the new phase occurs. In general, this type of phase transition is stochastic, heterogeneous, and complex, and there is a lack of a suitable method to probe the dynamics to establish the molecular level understanding of the process.

Electron microscopy (EM) and atomic force microscopy (AFM) have been promising approaches[9–13] in a wide range of systems. Yet, a state before the phase transition is often described as 'featureless' or 'amorphous' and the detailed description of how structural order emerges remains a key issue. Optical spectroscopy is a promising complementary approach to capture molecular dynamics during the early stage of nucleation. The stochastic, heterogeneous and complex nature of nucleation processes are, however, particularly detrimental to optical spectroscopy approaches.

This account highlights the unique optical microspectroscopy tools that we recently developed to study the emergence of morphology in various domains of research fields (Fig. 1). For ex-

*Correspondence: Dr. T. B. M. Adachi, E-mail: Takuji.Adachi@unige.ch
Dept. Physical Chemistry, University of Geneva, CH-1204 Geneva

ample, single crystal nucleation spectroscopy (SCNS) probes the crystallization process of one crystal nucleation at a time. SCNS in combination with theoretical calculations revealed molecular orders within aggregates that are typically described as 'amorphous'. SCNS setup can also be used as a laser tweezer Raman microspectroscopy tool to investigate the chemical nature of submicron objects diffusing in algal cells. Another development in the group is the time-resolved dynamic light scattering microscopy (micro-DLS). This method is promising in tracking the temporal evolution of the size distribution of nanoscale particles at the time resolution of tens of milliseconds. These techniques are label-free and non-invasive, and therefore their application in a wide range of systems is envisioned.

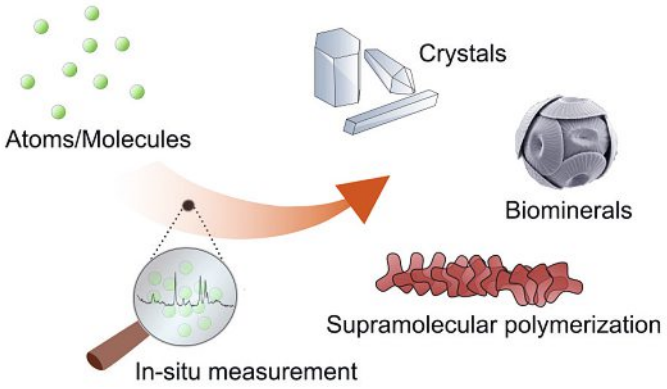

Fig. 1. We develop *in situ* optical spectroscopy to study the 'birth of morphology'. Image with clear background of *coccolithus pelagicus sp.* from ref [14].

2. Single Crystal Nucleation Spectroscopy (SCNS)

Crystallization is an important example where the nucleation process has been actively studied, and its molecular level understanding is crucial in a wide range of disciplines of science and industry, and even in our daily life.[1,3,15,16] Countless examples include the ice formation that impacts climate change, biomineralization that forms the beautiful shells of mollusks, but can also threaten our health by forming stones in kidneys, and during drug design and production in pharmaceuticals. The rational control and engineering of crystallization and its morphology have been limited by the lack of microscopic description of crystal nucleation. Crystallization, screening of crystal polymorphs, and the selection of crystal polymorphs have been performed based on trial-and-error approaches, which cost enormous amount of time and resources. Due to the stochastic nature of crystallization, statistical approaches, such as determining the nucleation rate under various crystallization conditions, have been the major experimental methods to develop crystal nucleation theory.[3,17] Recently, experimental approaches based on the cryo- and liquid cell transmission electron microscopy (TEM) have brought new insights on the crystal nucleation process.[9,10] The presence of morphologically 'featureless' or 'amorphous' clusters was confirmed in these TEM studies,[18,19] and *in situ* TEM results showed that these clusters became well-defined crystals.[20,21] More and more studies show the involvement of pre-nucleation aggregates in the crystal nucleation process and confirm the complexity of the crystal nucleation process in contrast to the classical nucleation theory.[18,20,22–25] The next critical steps toward establishing a microscopic picture include the detailed understanding of the structure of pre-nucleation aggregates that may form, how the crystalline order emerges from them, and how to rationally select polymorphism.[2,26]

Optical spectroscopy has a huge potential in extracting the molecular level details of the structural dynamics of pre-nucleation aggregates towards the phase transition. The application of optical spectroscopy on crystal nucleation problems has been, however, limited because the stochastic and heterogeneous nature of the nucleation process is particularly detrimental to the interpretation of the spectroscopic signals. If one probes a large volume of a sample to capture a nucleation event that can occur anywhere at any time, the spectroscopic signal from this nano-scale process would be buried in the average of various species in solution (*e.g.* monomers, aggregates, and crystals).

We reported a novel method, 'single crystal nucleation spectroscopy (SCNS)' to overcome this issue and spectroscopically probe crystallization processes one crystal nucleation at a time.[27] The SCNS is a method based on the combination of optical trapping induced crystallization (OTIC) and Raman microspectroscopy (Fig. 2a). When a continuous-wave (CW) laser beam is tightly focused into a solution, optical gradient force attracts particles toward the focus spot. Although the optical gradient force is not strong enough to trap a single molecule, crystallization eventually occurs at the focus spot and it has been assumed that the laser could increase the local concentration over time.[28] We use OTIC as a method to spatially control a single crystal nucleation event (*i.e.* at a focused laser spot), and the same laser generates Raman scattering allowing us to track the nucleation process one crystal nucleation at a time by Raman microspectroscopy (Fig. 2b). The polarization of our laser beam is depolarized to mimic natural crystallization. In our first report of SCNS, we demonstrated *in situ* Raman spectroscopy of single glycine crystallization from aqueous solution at 46 ms time resolution.[27]

Fig. 3a–f shows a series of Raman spectra obtained *in situ* during single crystal nucleation of glycine in aqueous solution. The dynamic nature of crystal nucleation can be observed. As a nucleation starts, broad Raman bands around 3200–3500 cm^{-1} first decreased (Fig. 3b). This is partially due to the increased local concentration of glycine molecules that pushed water molecules

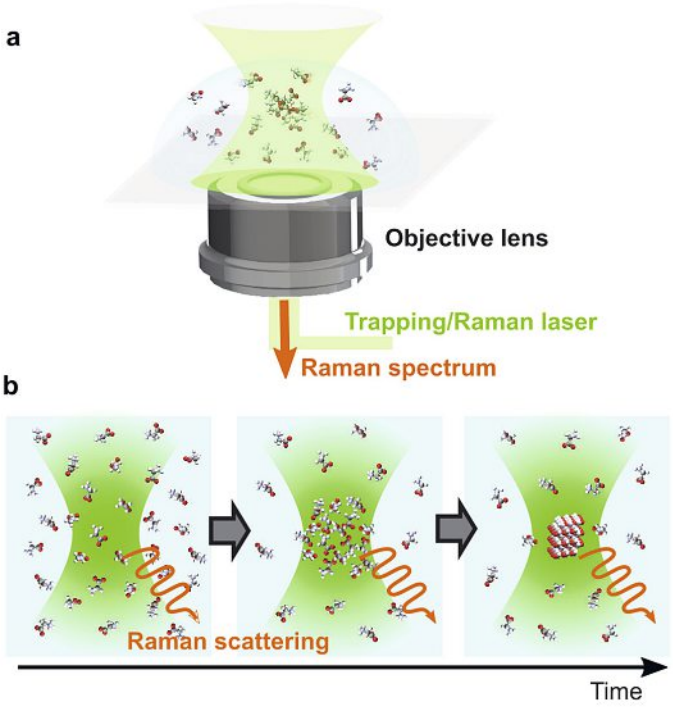

Fig. 2 a) A cartoon representing the dual role of 532 nm CW laser. A tightly focused CW laser induces crystallization at the focus while it serves as a Raman excitation laser to track the crystallization dynamics. b) A temporal representation of the molecular evolution under OTIC.[27]

out of the laser focus spot. This coincides with the appearance of a blurry object in the bright field image at the focus spot. The formation of a crystal is evidently captured with the increased Raman intensity and the appearance of new peaks (Fig. 3c), while the bright field image remains blurry. Among various spectral changes upon nucleation, the appearance of the Raman peak at 2954 cm^{-1} was of surprise because α-glycine (C-H stretching mode: ~2970 cm^{-1}) was the expected polymorph in water. The peak at 2954 cm^{-1} was assigned to be the formation of β-glycine. The spectral feature of β-glycine was short-lived and quickly became that of α-glycine (Fig. 3c–e).

The spectral evolution during a glycine nucleation was analyzed using non-negative matrix factorization (NMF),[29] a type of unsupervised principal component analysis (Fig. 3g–l). The advantage of this analysis is that the algorithm outputs a set of partial Raman spectrum (PRS) as well as the amplitude of each PRS without any assumption concerning their spectral shapes. The number of PRS is the only pre-determined parameter. A good quality fit was achieved with three PRS (Fig. 3g-k). PRS-1 and -2 match well with the Raman spectrum of solution and β-glycine, respectively. PRS-3, initially unidentified species could be assigned as the spectrum of pre-nucleation aggregates (see ref. [27] for details). The temporal evolution of each PRS amplitude (Fig. 3i) supported that glycine crystallization from water occurs in a non-classical nucleation pathway. Initially, the spectra were composed of 80–85 % of PRS-1, 0 % of PRS-2 and 15–20 % of PRS-3. Just before the nucleation occurred at ~2.65 s (the sudden increase of the PRS-2), the amplitude of PRS-1 decreased while that of PRS-3 increased (highlighted by grey color). Once a crystal formed, the amplitude of PRS-3 dropped to almost zero, suggesting that the pre-nucleation aggregates were converted to the crystal. This result was qualitatively reproduced in 33 experiments although there are some variances between each result due to the stochastic nature of crystallization. The *in situ* optical spectroscopic data at the single crystal nucleation level reveals how pre-nucleation aggregates form and convert to a crystal.

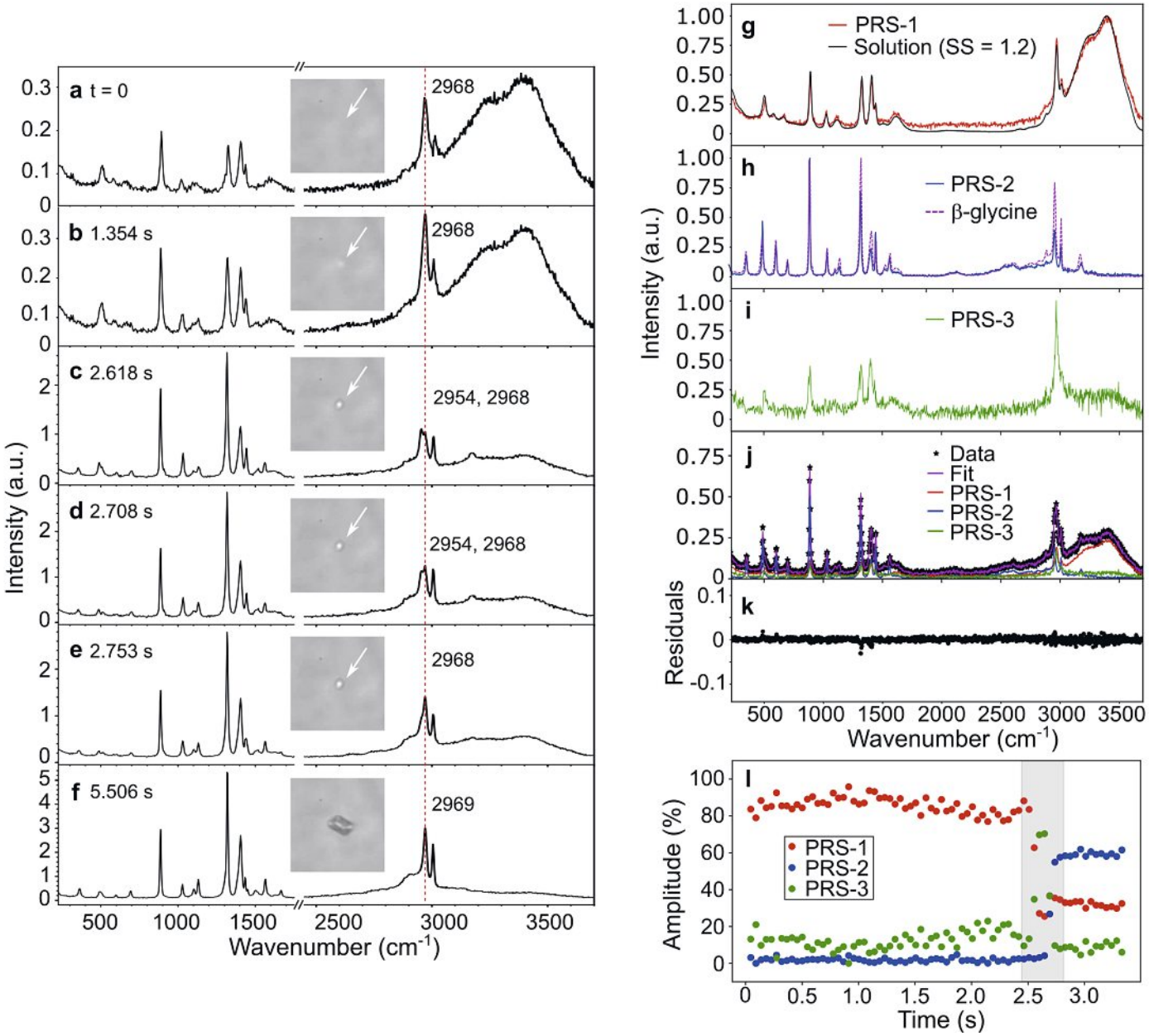

Fig. 3. a–f) Snapshots of Raman spectra of glycine in water showing the phase transition from solution (a) to crystal (f) with the corresponding bright field microscopy images (16x16 μm) as insets. g–i) Three spectra obtained by non-supervised data decomposition of the series of spectra during crystal nucleation (PRS: Partial Raman Spectrum 1–3). j) An example of the fit to the data by three constituents and k) the residuals of the fit. l) Temporal evolution of each constituent amplitude during the crystal nucleation.[27]

SCNS further identified the Raman spectrum of pre-nucleation aggregates for the first time. This is a key experimental observable that SCNS can uniquely provide. Using the spectral feature as a bridge, the experimental Raman spectrum of pre-nucleation aggregates was compared with the simulated spectra of glycine aggregates from molecular dynamics simulation. The comparison led us to propose that the emergence of the order occurs *via* formation of hydrogen-bonded linear networks.

This work demonstrated that SCNS can not only extract the information of crystal nucleation pathways (classical *vs* non-classical), but also reveal the polymorph conversion process, even if the lifetime of meta-stable polymorph is too short to be detected by conventional bulk characterization tools. This is a crucial advantage in studying the effect of environment (different solvents, the presence of additives *etc.*) on crystal nucleation pathways. In the case of glycine, for example, the addition of salts in aqueous solution results in the formation of γ-glycine. In literature, a proposed mechanism is that ions disrupt cyclic dimers of glycine and form a linear chain to build γ-glycine.[30] Our work showed that glycine forms hydrogen-bonded linear chains instead of cyclic dimers even in pure water. It is now exciting to study the role of salts on the glycine crystallization pathway using SCNS.[31] A similar question is posed in many different systems including active pharmaceutical ingredients (APIs). We foresee that SCNS will become a powerful tool to elucidate the effect of various chemical environments on the early stage of crystallization at the molecular level so that rational polymorph selection is realized.

3. Laser Tweezer Raman Microspectroscopy for *in vivo* Investigation of Biomineralization

Biomineralization is a fascinating process by which living organisms produce minerals. From the simplest unicellular to the most complex organism, biomineralization covers a wide range of formation mechanisms, which can explain the function and structure of biominerals. In various biological systems, minerals can be used as protection or internal structure such as skeletons of corals, shells, and vertebrates. In these cases, the process of mineralization (composition, nucleation, growth, morphology and location) is controlled by cellular activities and is called biologically controlled mineralization.[32,33] In others, mineralization can be induced by secondary reactions leading to favorable conditions to form a mineral such as kidney stones. This type of process, called biologically induced mineralization,[32,33] results in heterogeneity in size, shape and composition of the mineral phase as there is no control from the organism.

Barium sulfate, or barite, is a heavy biomineral, the presence of which in organisms is still poorly understood. Indeed, barium has the particularity of being highly toxic under its ionic form, while holding the lowest solubility among sulfate salts.[34] Firstly, one hypothesized that it could serve as gravity sensing, as studied in freshwater green algae, Chara.[35] The use of barium sulfate crystals as statolith was then applied to *Closterium*, *Micrasterias* and *Spirogyra*[36–40] (freshwater green algae from *Zygnematophyceae*), as they are motile in water.[39] Recently, studies point towards the toxicity of barium.[36,37] For example, Krecji *et al.* found that the terminal vacuoles of *Closterium* contained high sulfate concentrations, which could act as a trap to precipitate barium and isolated it from the rest of the cell.[37] According to these authors, *Closterium* adopts the detoxification mechanism to decrease the concentration of barium throughout the cell as they observed that transport proteins do not discriminate between Ca, Ba and Sr. Currently, there is no leading evidence to conclude the reason why species among this class of green algae present barite microcrystals inside their cells.

Among various freshwater algae, we chose *Spirogyra* for our study because this alga is the least studied regarding the microcrystal formation while it is widely used as a model organism to study the algal system. Its size and transparency make the species relatively easy to observe under optical microscopy and its genus is clearly recognized because of its helical chloroplasts (Fig. 4a). Our study focused on the description and localization of these crystals within *Spirogyra* combining *in vitro* electron microscopy and *in vivo* laser tweezer Raman microspectroscopy.[41] From these results, a formation mechanism was proposed, which will help hopefully to answer if these crystals play a biological role in *Spirogyra* or not.

The characterization of the size, morphology and composition of microcrystals was first performed *in vitro* on simple dried cells with scanning electron microscopy (SEM) and energy-dispersive X-ray spectroscopy (EDXS) (Fig. 4b). Within *Spirogyra* cells, crystal sizes varied from 300 to 500 nm for the smallest and 700 nm to 1 μm for the largest. EDXS analysis indicated that these crystals consisted of Ba and S, suggesting that they are barite. The crystal shapes ranged from rounded to hexagonal and rhombohedral. Fig. 4b shows mainly rhombohedral crystals with (210) and (001) faces, meanwhile a hexagonal crystal with the (011) is presented in Fig. 4d. (011) face is rarely seen in synthetic barite crystals because of its fast growth rate.[42] The observation of (011) face is most likely due to organic molecules in cells (*e.g.* phosphonates, carboxylates) influencing the crystal habit.[42–46]

SEM-EDXS analyses were also conducted on the samples dried *via* the critical point drying process to preserve the cell

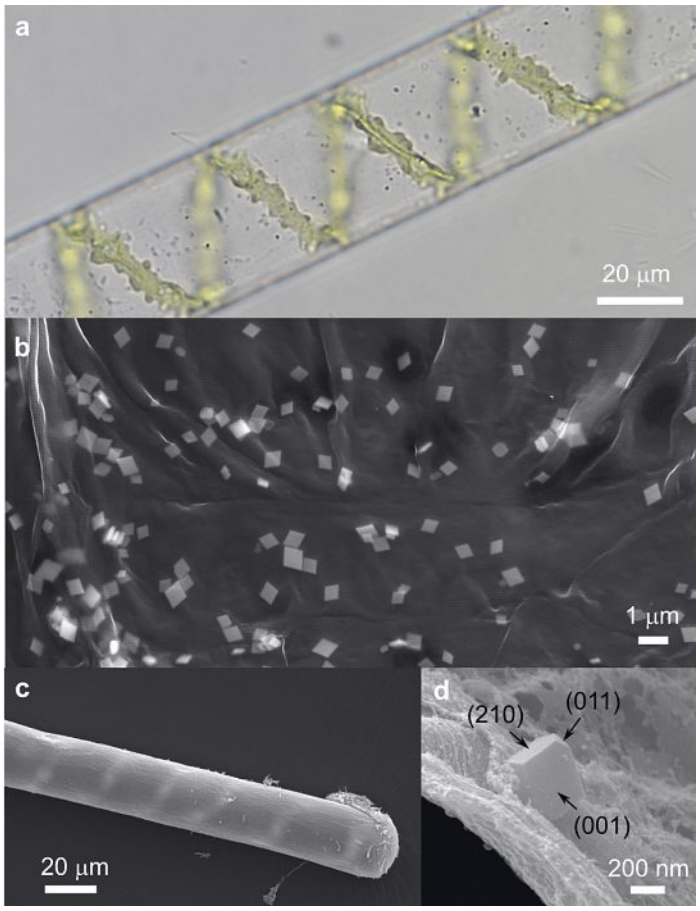

Fig. 4. a) Optical image of a *Spirogyra* cell focused on the bottom of the cell, where small particles are visible. b) SEM image of barite crystals inside a simply dried cell of *Spirogyra* using SEM. c) SEM images of *Spirogyra* cells prepared by the critical point drying method. End cell of a preserved filament, where the helical chloroplast is visible from inside the cell. d) Zoomed image on a barite crystal inside a preserved cell. A rhombohedral barite crystal is observed with crystallographic faces (210) and (001). From the cleavage of these two faces, a fast-growing face (011) can appear and is present in the hexagonal crystals.[41]

structure for investigating the location of barite microcrystals (Fig. 4c–d). Fig. 4c illustrates that the samples, after undergoing critical point drying, retained the cylindrical form of the cell and the spiral arrangement of *Spirogyra* chloroplasts, appearing brighter below the cell wall. Vacuole contents dried up during the drying procedure, but the vestige of its presence was observed through the maintained chloroplasts and the cytoplasmic membrane pushed against the cell wall (see ref. [41] for details). Fortunately, a few damaged cells revealed their internal structure, making it possible to identify the different organelles (chloroplasts, cytoplasmic membrane *etc.*) and the neighboring environment of barite crystals. Fig. 4d is a magnified image of a crystal found inside the cell, where cytoplasmic membrane can be seen under and behind the crystal. The cell is delimited by the cell wall, also present under the cytoplasmic membrane (Fig. 4d). We could also observe that the crystals found in this broken cell were in contact with chloroplasts and a fibrillary network. This network might consist of either actin filaments or accumulations of other biochemical substances formed during the water removal process in critical point drying. Given the presence of barite microcrystals within the cytoplasmic membrane and chloroplasts, our findings provide support that barite crystals exist within the protoplast.

These findings from *in vitro* approach were then combined with *in vivo* optical microscopy and Raman microspectroscopy to identify their location within living cells. While examining *Spirogyra* cells, none of the immobile objects displayed the characteristic Raman spectrum of barite. Instead, multiple mobile particles were noticed when focusing on the cell's upper or lower regions. These particles could be stably trapped optically at the bottom of the cell (Fig. 5a–f), allowing the acquisition of their Raman spectra (Fig. 5g). Remarkably, these spectra closely matched the Raman spectrum of synthetic barite. This result not only allowed us to identify the composition of the particles, which agrees with EDX analysis, but also to confirm the optical visibility of barite crystals and their placement within the cytoplasm. Moreover, these crystals exhibited mobility.

To determine the distribution of barite crystals within a cell, optical microscopy images were captured at various heights along the z-axis.[41] Mobile barite crystals were observed at the bottom, top, sides, and around the nucleus of *Spirogyra* cells, indicating their presence in the cytoplasm near the cell walls. This observation aligned with the Raman spectrum of barite particles often detected at the bottom of a cell above the cell wall. Observing their motion revealed that the microcrystals move in the direction of cytoplasmic streaming, a rapid cellular movement driven by actin filaments and myosin motor proteins.[47] This intricate motion of barite crystals suggests a complexity beyond Brownian motion and supports their presence in the cytoplasm of living *Spirogyra* cells.

Based on these findings, we proposed that the formation of barium sulfate occurs within the cytoplasm, where the necessary conditions for precipitation can be met. This involves, firstly, non-selective transport of Ba^{2+} ions, observed in *Closterium*,[37] alongside the active transportation of divalent cations like Ca^{2+} and Mg^{2+}, needed for actin polymerization.[48] Secondly, chloroplasts assimilate sulfate for amino acid biosynthesis,[49] implying its presence in the cytoplasm. Whether barite precipitation in *Spirogyra* is a result of biologically induced processes or a controlled biomineralization process remains an unanswered question.

This work demonstrates the advantage of *in vivo* optical microspectroscopy to characterize the chemical nature of microcrystals within living cells. The combination of *in vivo* approaches with *in vitro* SEM and EDXS studies that are typically used in biology can significantly advance our understanding of barite biomineralization in *Spirogyra*. As the laser tweezer Raman microspectroscopy is non-invasive, it has a potential to be applied in a variety of systems.[50–52] Further research will be conducted to answer the question whether barite microcrystals have a biological role in *Spirogyra*.

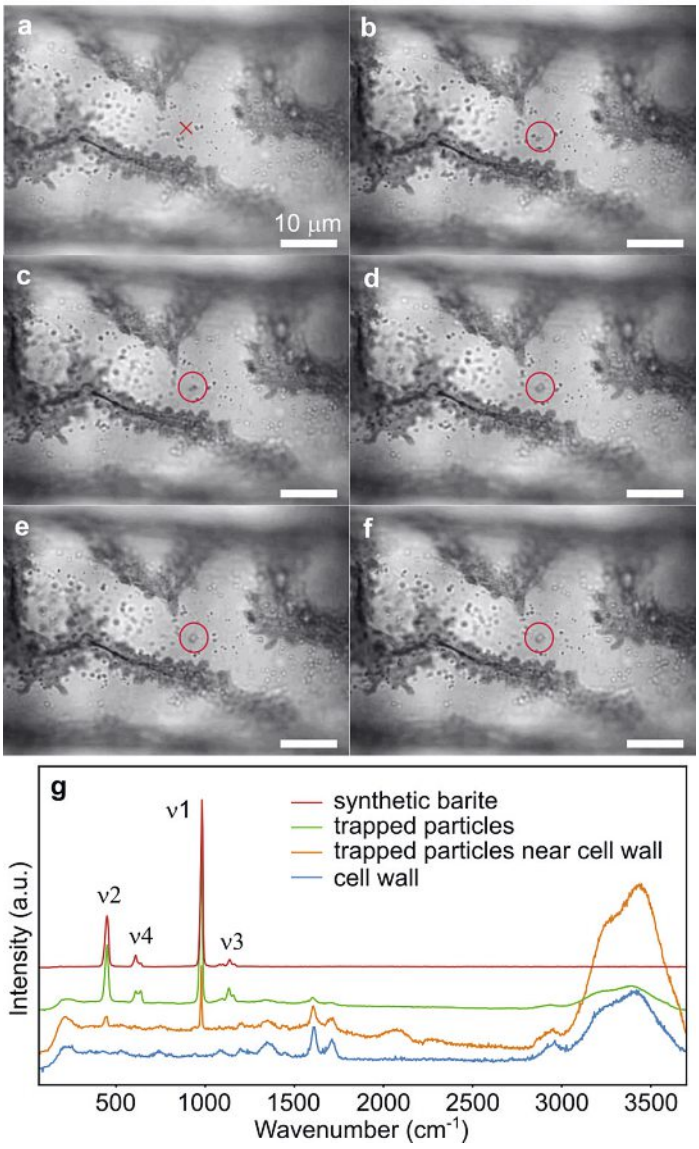

Fig. 5. a–f) Successive optical microscopy images of living *Spirogyra* cell during laser tweezer Raman microspectroscopy. Interval time between each panel is 0.5 s. a) Representation of the focus point of the laser by a red cross. b–f) Particles were attracted towards the laser focus and formed an aggregate seen as a bigger particle (red circle). g) Raman spectra of the cell wall trapped particles near and far from the cell wall, and synthetic barite. The trapped particles show distinct Raman peaks matching those of synthetic barite.[41]

4. Time-resolved Dynamic Light Scattering Microscopy (micro-DLS)

While expanding the application of our microspectroscopy tools, we realized that systems relevant to biomineralization such as barium sulfates or calcium carbonates present extremely low solubilities in water (~μg/ml) and precipitate quickly. This prevents us from using SCNS to study crystal nucleation process of barium sulfates or calcium carbonates one crystal nucleation at a time, because it is practically impossible to hold the system in a metastable state for long enough to induce crystallization by optical gradient forces. On these systems, we are forced to monitor a large number of crystal nucleation events, yet there is a lack of tools that can monitor the temporal evolution of their morphology and structure simultaneously at a reasonable time resolution.[6] For example, structural information can be monitored by Ra-

man microspectroscopy at a reasonable time resolution, but it is not easy to follow the size evolution of systems in time-resolved manner. The use of synchrotron source to perform small-angle and wide-angle X-ray diffraction (SAXS and WAXS) may be an option to follow the size evolution at 100 ms time resolution *in situ*,[53] but the accessibility to the resources is limited.

Dynamic Light Scattering (DLS) has been an established method for several decades in assessing the size of nano-objects within colloidal solutions, finding application in diverse fields including colloid and polymer sciences, food chemistry, nanotechnology, nanomedicine, and biomedical research.[54–59] DLS is a photon correlation spectroscopy, based on the fluctuation of light intensity generated by the interference of single scatterings from colloidal particles that are undergoing Brownian motion.[60] The intensity fluctuation is analyzed by an autocorrelation function, and the diffusion coefficient of the particles can be extracted from the decay of autocorrelation curve. The broad utility of DLS is derived from its non-destructive capability to provide ensemble particle size estimates across a wide size range, and its use is relatively quick and easy.[59] A conventional DLS setup is composed of a coherent light source and a photodetector, positioned in a manner that optically links them to the sample. The photodetector is connected to a data acquisition module (correlator), allowing high acquisition rates necessary for capturing fluctuations from particle dynamics (Fig. 6a).

However, a major limitation of conventional DLS is a long acquisition time needed for constructing autocorrelation curves, which typically could take up to several minutes. Thus, the size distribution of a sample must stay unchanged during the measurement. This makes DLS as a tool to characterize the size distribution of samples in steady-state, while one of the important information for studying crystallization is the temporal evolution of the size distribution.

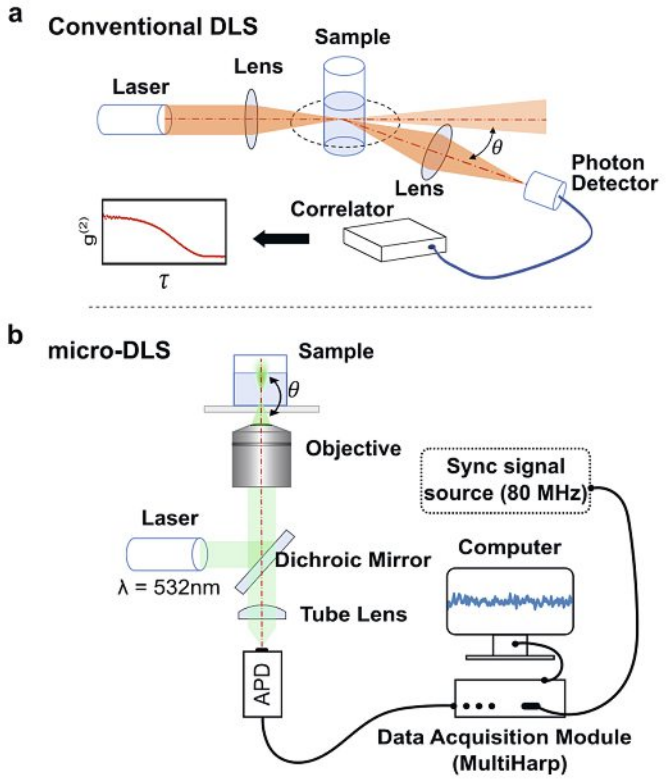

Fig. 6. Schematic diagrams summarizing the setup arrangement and its main component of a) an example of the conventional DLS and b) micro-DLS built in our group. The use of TCSPC module enables a post data analysis.

To this end, we have developed time-resolved dynamic light scattering microscopy (micro-DLS).[61,62] The implementation of DLS on a microscopy system had been previously reported.[63,64] In these reports, micro-DLS was developed to overcome other limitations of conventional DLS which cannot measure the size of opaque (highly concentrated) samples and is vulnerable to the presence of contaminants (such as large dust particles). It offers a substantially enhanced spatial resolution, enabling localized measurements in heterogeneous materials and improving DLS performance when dealing with contaminants.[63] Additionally, it excels in analyzing opaque samples characterized by high light-scattering and light-absorbing properties.[64] The setup developed in our group employs a back-scattering arrangement, a confocal optical design, and the partial heterodyne correction of the detected signal.[64]

Upon development of the time-resolved micro-DLS, we chose to build a post data processing program rather than a program that calculates autocorrelation on the fly. The advantages of post data processing strategy has been demonstrated for excluding pollutants[65] and improving the precision and accuracy of measured size distributions,[66] for example. The flexibility in selecting time ranges of interest significantly improves the DLS capabilities in tracking dynamic chemical processes *in situ*.

The simple scheme of micro-DLS setup with post data processing capabilities is shown in Fig. 6b.[61] The optical setup is basically a confocal microscope, where a CW laser is focused on a solution sample using an objective lens and the scattering signal is collected by the same lens and detected using an avalanche photodiode (APD). The arrival time of each photon is registered using time-correlated single photon counting (TCSPC) devices. This is crucial for the post data processing. As a CW laser is used for the measurement, an external synchronization signal operating at 80 MHz was employed for the time-tag reference. Confocal alignment is crucial in micro-DLS as it removes the effect of multiple scattering to keep the amplitude of autocorrelation high.

On the software side, an in-house Python program was written for the post data analysis.[61] The program can load the data and display first the scattering intensity as function of time at arbitrarily chosen time bins. A user is free to slice the data within a specific range. The sliced data is then used to calculate the second order normalized autocorrelation function (ACF). The second order ACF was calculated from photon arrival times by adopting a coincidence counting algorithm developed in the field of single molecule spectroscopy,[67] instead of using intensity counts. This algorithm is the key for constructing ACF from a limited number of photons. Using the obtained ACF, the distribution of diffusion coefficients was computed by solving an inversion problem by regularized non-negative least squares with Tikhonov regularization.[61]

Firstly, we assessed whether our system is capable of accurately determining the monomodal size distribution of a colloidal solution. We used a solution of polystyrene beads of 60 nm at 0.1 wt.% and a solution of 220 nm at 5 wt.% (Fig. 7) and measured the scattering from each sample (Fig. 7a–b). Following the post data analysis method mentioned above, we computed the ACF from a time window width of 180 s (Fig. 7c–d) and reconstructed the size distribution (Fig. 7e–f). The size distribution shown in Fig. 7e–f indicates that the micro-DLS setup with the post data processing works as good as a commercial DLS setup to estimate the correct size distribution of monomodal colloidal solutions. The size distribution was fitted to a log-normal function and gave the peak s_0 = 69 nm and full width at half maximum (FWHM) = 54 nm for 60 nm particles, and s_0 = 264 nm and FWHM = 226 nm for 220 nm particles, respectively. The size distribution from the commercial DLS was s_0 = 75 nm and FWHM = 51 nm for 60 nm particles, and s_0 = 300 nm and FWHM = 303 nm for 220 nm particles, respectively. Further detailed characterization of

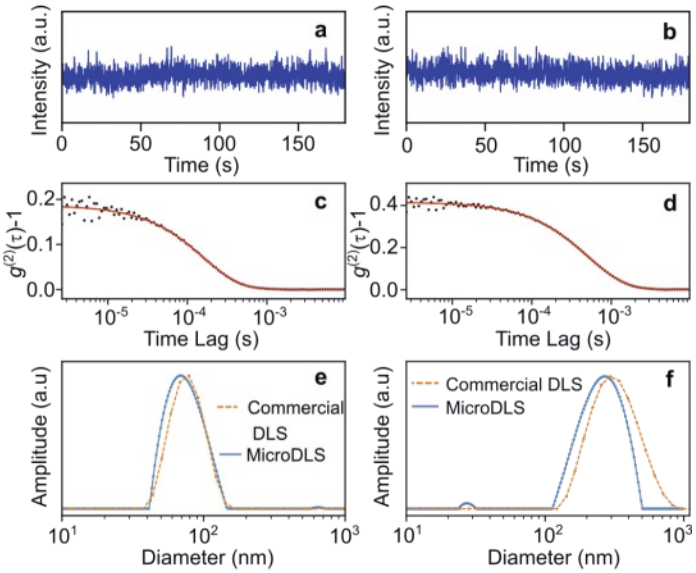

Fig. 7. Measurements of monomodal size distributions from two samples containing 60 nm (0.1 wt.%), panels (a, c, e), and 220 nm (5 wt.%) polystyrene particles, panels (b, d, f). a–b) Time evolution of binned counts for each measurement. c–d) Computed ACF (dots) and the reconstructed fit (solid line), with a time span of 180 s. e–f) Reconstructed size distribution from the micro-DLS (blue solid line) and a commercial DLS (orange dashed line).[61]

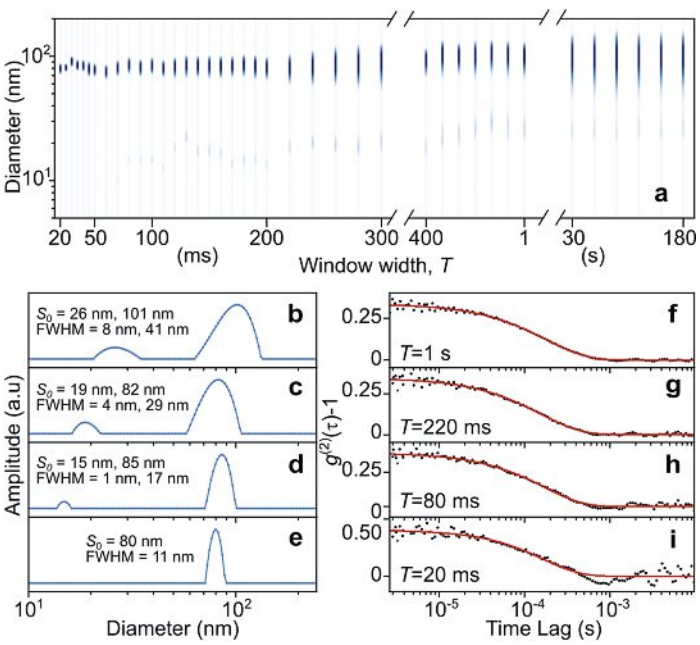

Fig. 8. The size distribution of a solution mixture of 20 nm silica particles and 80 nm polystyrene particles. a) Two-dimensional plot of the size distribution reconstructed using different time window width, *T*. The size distributions for b) *T* = 1s, c) 220 ms, d) 80 ms, and e) 20 ms, with reported values from log-normal fit. f–i) ACF (dots) and the reconstructed fit (solid line) for each of the size distributions in b–e).[61]

the setup and analysis were performed and can be found in our previous reports.[61,62]

The important question on this development was to address what the shortest time window outputting the correct size distribution would be. The first test was performed by fixing the initial point of the time window and varied its width from 180 s to 20 ms. A mixed solution of 20 and 80 nm nanoparticles was used for this measurement. Fig. 8a is a two-dimensional plot where the amplitude of the size distribution is represented by the opacity of the color for a series of time window width, *T*, (180 s to 20 ms). Fig. 8b–e show the size distribution at *T* = 1 s, 220 ms, 80 ms and 20 ms, respectively. Fig. 8f–i are the corresponding ACF that were used for constructing the size distribution shown in Fig. 8b–e. While *T* was reduced until 80 ms, the bimodal distribution with reasonable size range was extracted. Below this *T*, the distribution corresponding to 20 nm colloidal solution was no longer detected (*cf.* Fig. 8e, *T* = 20 ms). The quality of ACF is also poor when *T* = 20 ms (Fig. 8i). Based on this analysis, we concluded that the smallest time window width to properly characterize the size distribution was 80 ms under these experimental conditions.

An interesting outcome from the analysis based on a short time window width is the variation of FWHM of the size distributions. Typically, when large *T* (> 30 s) is used, FWHM of the size distribution tends to broaden. When the shorter T is used, FWHM reduces significantly (Fig. 8a). Narrow distributions observed at the shorter *T* were attributed to the capability of time-resolved micro-DLS to undercover the sub-ensemble of a broad size distribution.[61] Indeed, there is inherently some polydispersity of the particle size when a colloidal solution is prepared. When long *T* is used for calculating ACF, it represents an average of all the particle sizes in ensemble and therefore the reconstructed size distribution is broad. Also, larger particles contribute to scattering more than smaller ones, and therefore the size distribution is somewhat biased toward larger sizes. We have tested this hypothesis by reconstructing the distribution from consecutive 80 ms windows over 180 s time span (Fig. 9). From single 80 ms span, the peak of the size distribution varied between window positions, but it stayed under the broad distribution obtained by the *T* = 180 s window (Fig. 9a). One can construct the size distribution by accumulating the sub-ensemble (Fig. 9b). The result matched the specification of the colloidal solution better (with a smaller FWHM), than when one window of *T* = 180 s was used for estimating the size distribution.

The time-resolved micro-DLS can extract the size of colloidal solution every 80 ms. The improvement of temporal resolution of DLS is several orders of magnitude compared with a commercially available DLS. This is a breakthrough as it opens the application of DLS to systems that temporally evolve. As the setup was developed around a microscopy environment, the combination with other spectroscopic methods can be easily implemented. The analysis software allows users to customize the window width and position for reconstructing size distributions. This flexibility is a crucial aspect of our micro-DLS, as it makes it easy to correlate the size evolution with the temporal change of spectroscopic data when micro-DLS is combined with other spectroscopic measurement. The combination of microspectroscopy and micro-DLS may be able to simultaneously provide both structural and morphological information during the early stages of barium sulfate or calcium carbonate precipitation, and furthermore a wide range of systems such as supramolecular polymers and protein self-assembly may be studied.

5. Conclusions

This account highlighted our recent works on developing *in situ/in vivo* optical microspectroscopy to study the emergence of morphology. The understanding of how molecules form nucleus and evolve into different morphology at the molecular level is of great importance in a wide range of scientific disciplines. Although, optical spectroscopy is an ideal tool for probing molecular dynamics, it has been rarely used to tackle this problem. We have established two platforms, SCNS and time-resolved micro-DLS, which are both label-free and non-invasive. SCNS can also be used as a laser tweezer Raman microspectroscopy for *in vivo* study of biological systems. Both systems are similar to a simple confocal microscope and so far, only one laser beam is needed. This suggests that these setups can be further tailored by

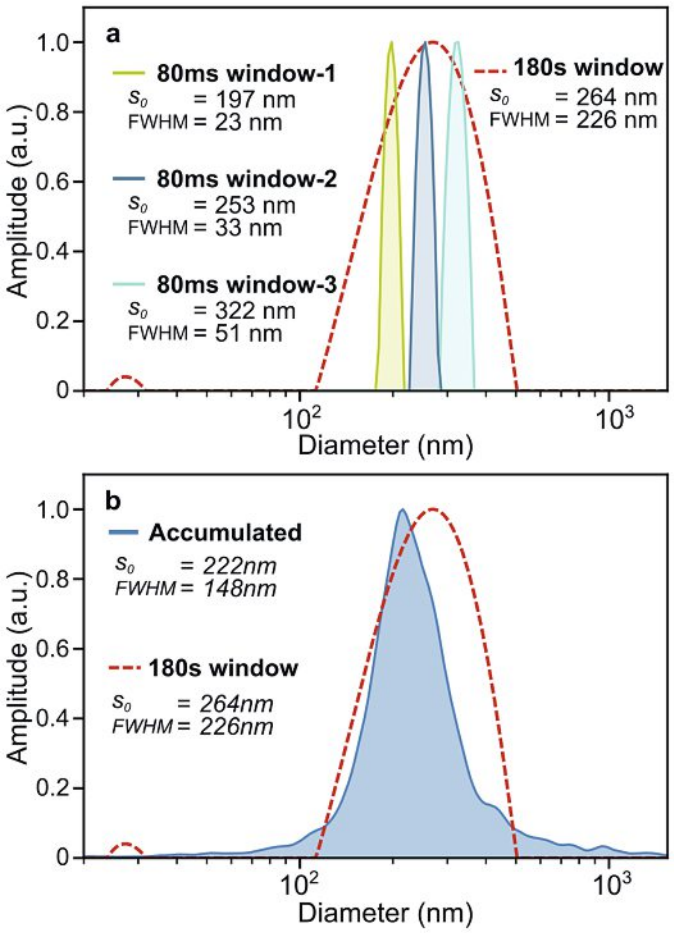

Fig. 9. Comparison of normalized size distributions of a 220 nm polystyrene solution. a) Three examples of size distributions obtained from single 80 ms time windows, compared to the size distribution from a single 180 s time window. b) The accumulation of consecutive 80 ms time windows over a 180 s time period, compared to the size distribution from a single 180 s time window.[61]

combining them with other spectroscopic tools depending on the type of desired *in situ* information. There are plenty of interesting problems in various scientific fields where the development of time-resolved *in situ/in vivo* spectroscopy tools is needed. The ongoing advancement of *in situ/in vivo* optical microspectroscopy will provide strong impetus for accelerating our ability to understand and control the early stage of morphological formation at the molecular level.

Acknowledgements

We acknowledge the University of Geneva for financial support.

Received: November 30, 2023

[1] J. W. Mullin, 'Crystallization', Butterworth-Heinemann, Oxford; Boston, **2001**.
[2] R. J. Davey, S. L. M. Schroeder, J. H. ter Horst, *Angew. Chem. Int. Ed.* **2013**, *52*, 2166, https://doi.org/10.1002/anie.201204824.
[3] G. C. Sosso, J. Chen, S. J. Cox, M. Fitzner, P. Pedevilla, A. Zen, A. Michaelides, *Chem. Rev.* **2016**, *116*, 7078, https://doi.org/10.1021/acs.chemrev.5b00744.
[4] T. F. A. De Greef, M. M. J. Smulders, M. Wolffs, A. P. H. J. Schenning, R. P. Sijbesma, E. W. Meijer, *Chem. Rev.* **2009**, *109*, 5687, https://doi.org/10.1021/cr900181u.
[5] C. Kulkarni, E. W. Meijer, A. R. A. Palmans, *Acc. Chem. Res.* **2017**, *50*, 1928, https://doi.org/10.1021/acs.accounts.7b00176.
[6] A. Dey, G. de With, N. A. J. M. Sommerdijk, *Chem. Soc. Rev.* **2010**, *39*, 397, https://doi.org/10.1039/B811842F.
[7] S. Weiner, L. Addadi, *Annu. Rev. Mater. Res.* **2011**, *41*, 21, https://doi.org/10.1146/annurev-matsci-062910-095803.
[8] E. M. Avrahami, L. Houben, L. Aram, A. Gal, *Science* **2022**, *376*, 312, https://doi.org/10.1126/science.abm1748.
[9] F. M. Ross, *Science* **2015**, *350*, aaa9886, https://doi.org/10.1126/science.aaa9886.
[10] J. J. De Yoreo, S. N. A. J. M., *Nat. Rev. Mater.* **2016**, *1*, 16035, https://doi.org/10.1038/natrevmats.2016.35.
[11] T. Fukui, T. Uchihashi, N. Sasaki, H. Watanabe, M. Takeuchi, K. Sugiyasu, *Angew. Chem. Int. Ed.* **2018**, *57*, 15465, https://doi.org/10.1002/anie.201809165.
[12] B. Jin, Z. Liu, R. Tang, *Cryst. Eng. Comm.* **2020**, *22*, 4057, https://doi.org/10.1039/D0CE00480D.
[13] A. Rizvi, J. T. Mulvey, B. P. Carpenter, R. Talosig, J. P. Patterson, *Chem. Rev.* **2021**, *121*, 14232, https://doi.org/10.1021/acs.chemrev.1c00189.
[14] Y. Jeremy, 'Coccolithus pelagicus ssp. pelagicus', Plankton*Net Data Provider at the Alfred Wegener Insitute for Polar and Marine Research, hdl: 10013/de.awi.planktonnet.
[15] R. Tamura, M. Miyata, 'Advances in Organic Crystal Chemistry Comprehensive Reviews 2015', Springer, Tokyo, **2015**.
[16] J. Bernstein, 'Polymorphism in molecular crystals', Oxford University Press, OxfordClarendon Press; New York, **2002**.
[17] J. W. Mullin, 'Crystallization', Elsevier Science, Jordan Hill, **2014**.
[18] Y. Tsarfati, S. Rosenne, H. Weissman, L. J. W. Shimon, D. Gur, B. A. Palmer, B. Rybtchinski, *ACS Cent. Sci.* **2018**, *4*, 1031, https://doi.org/10.1021/acscentsci.8b00289.
[19] R. E. Schreiber, L. Houben, S. G. Wolf, G. Leitus, Z.-L. Lang, J. J. Carbó, J. M. Poblet, R. Neumann, *Nat. Chem.* **2016**, *9*, 369, https://doi.org/10.1038/nchem.2675.
[20] T. Yamazaki, Y. Kimura, P. G. Vekilov, E. Furukawa, M. Shirai, H. Matsumoto, A. E. S. Van Driessche, K. Tsukamoto, *Proc. Natl. Acad. Sci. U.S.A.* **2017**, *114*, 2154, https://doi.org/10.1073/pnas.1606948114.
[21] T. Nakamuro, M. Sakakibara, H. Nada, K. Harano, E. Nakamura, *J. Am. Chem. Soc.* **2021**, *143*, 1763, https://doi.org/10.1021/jacs.0c12100.
[22] D. Erdemir, A. Y. Lee, A. S. Myerson, *Acc. Chem. Res.* **2009**, *42*, 621, https://doi.org/10.1021/ar800217x.
[23] D. Gebauer, M. Kellermeier, J. D. Gale, L. Bergström, H. Cölfen, *Chem. Soc. Rev.* **2014**, *43*, 2348, https://doi.org/10.1039/C3CS60451A.
[24] M. Jehannin, A. Rao, H. Cölfen, *J. Am. Chem. Soc.* **2019**, *141*, 10120, https://doi.org/10.1021/jacs.9b01883.
[25] P. G. Vekilov, *Nanoscale* **2010**, *2*, 2346, https://doi.org/10.1039/c0nr00628a.
[26] S. Price, S. Veesler, H. Pan, K. Lewtas, M. Smets, B. Rimez, A. Myerson, C. Hughes, A. Hare, F. Zhang, H. Meekes, M. Mazzotti, I. Rosbottom, D. Khamar, J. van den Ende, L. Fabian, S. Black, F. Taulelle, M. Gich, P. Vekilov, D. Toroz, C. A. Bertran, J. Sefcik, S. Schroeder, S. Booth, A. Rasmuson, E. Breynaert, E. Simone, R. Hammond, R. Sear, J. de Yoreo, R. Davey, J. Anwar, R. Ristic, D. M. Camacho Corzo, K. Roberts, K. Harris, H. Colfen, T. Turner, *Faraday Discuss.* **2015**, *179*, 155, https://doi.org/10.1039/C5FD90036K.
[27] O. Urquidi, J. Brazard, N. LeMessurier, L. Simine, T. B. M. Adachi, *Proc. Natl. Acad. Sci. U.S.A.* **2022**, *119*, e2122990119, https://doi.org/10.1073/pnas.2122990119.
[28] T. Sugiyama, T. Adachi, H. Masuhara, *Chem. Lett.* **2007**, *36*, 1480, https://doi.org/10.1246/cl.2007.1480.
[29] W. Woelffel, C. Claireaux, M. J. Toplis, E. Burov, É. Barthel, A. Shukla, J. Biscaras, M.-H. Chopinet, E. Gouillart, *J. Non-Cryst. Solids.* **2015**, *428*, 121, https://doi.org/10.1016/j.jnoncrysol.2015.08.016.
[30] X. Yang, J. Lu, X.-J. Wang, C.-B. Ching, *J. Cryst. Growth* **2008**, *310*, 604, https://doi.org/10.1016/j.jcrysgro.2007.11.072.
[31] B. Peters, *Proc. Natl. Acad. Sci. U.S.A.* **2022**, *119*, e2204971119, https://doi.org/10.1073/pnas.2204971119.
[32] H. A. Lowenstam, *Science* **1981**, *211*, 1126, https://doi.org/10.1126/science.7008198.
[33] S. Mann, 'Biomineralization Principles and Concepts in Bioinorganic Materials Chemistry', Oxford University PressOxford, **2001**, https://doi.org/10.1093/oso/9780198508823.001.0001.
[34] P. L. Brown, C. Ekberg, A. V. Matyskin, *Geochim. Cosmochim. Acta* **2019**, *255*, 88, https://doi.org/10.1016/j.gca.2019.04.009.
[35] K. Schröter, A. Läuchli, A. Sievers, *Planta* **1975**, *122*, 213, https://doi.org/10.1007/BF00385269.
[36] U. Meindl, *Phyton (Horn)* **1984**, *24*, 273, https://doi.org/10.1007/978-3-0348-9314-5_3
[37] M. R. Krejci, B. Wasserman, L. Finney, I. McNulty, D. Legnini, S. Vogt, D. Joester, *J. Struct. Biol.* **2011**, *176*, 192, https://doi.org/10.1016/j.jsb.2011.08.006.
[38] M. Niedermeier, N. Gierlinger, U. Lütz-Meindl, *J. Plant Physiol.* **2018**, *230*, 80, https://doi.org/10.1016/j.jplph.2018.08.008.
[39] A. J. Brook, A. Fotheringham, J. Bradly, A. Jenkins, *Brit. Phycol. J.* **1980**, *15*, 261, https://doi.org/10.1080/00071618000650251.

[40] D. R. Kreger, H. Boeré, *Acta Bot. Neerl.* **1969**, *18*, 143, https://doi.org/10.1111/j.1438-8677.1969.tb00579.x.
[41] N. Barbosa, J.-M. Jaquet, O. Urquidi, T. B. M. Adachi, M. Filella, *J. Plant Physiol.* **2022**, *276*, 153769, https://doi.org/10.1016/j.jplph.2022.153769.
[42] S. N. Black, L. A. Bromley, D. Cottier, R. J. Davey, B. Dobbs, J. E. Rout, *J. Chem. Soc., Faraday trans.* **1991**, *87*, 3409, https://doi.org/10.1039/ft9918703409.
[43] W. J. Benton, I. R. Collins, I. M. Grimsey, G. M. Parkinson, S. A. Rodger, *Faraday Disc.* **1993**, *95*, 281, https://doi.org/10.1039/fd9939500281.
[44] E. Barouda, K. D. Demadis, S. R. Freeman, F. Jones, M. I. Ogden, *Cryst. Growth Des.* **2007**, *7*, 321, https://doi.org/10.1021/cg0604172.
[45] E. Mavredaki, A. Neville, K. S. Sorbie, *Cryst. Growth Des.* **2011**, *11*, 4751, https://doi.org/10.1021/cg101584f.
[46] E. D. Athanasopoulos, E. Armakola, P. G. Koutsoukos, K. D. Demadis, *CrystEngComm* **2018**, *20*, 6589, https://doi.org/10.1039/C8CE01116H.
[47] R. Wayne, 'Plant cell biology: from astronomy to zoology', Academic Press, An Imprint Of Elsevier, London, United Kingdom; San Diego, CA, United States, **2019**.
[48] J. E. Estes, L. A. Selden, H. J. Kinosian, L. C. Gershman, *J. Muscle Res. Cell. Motil.* **1992**, *13*, 272, https://doi.org/10.1007/BF01766455.
[49] A. Melis, H.-C. Chen, *Photosynth. Res.* **2005**, *86*, 299, https://doi.org/10.1007/s11120-005-7382-z.
[50] D. V. Petrov, *J. Opt. A: Pure Appl. Opt.* **2007**, *9*, S139, https://doi.org/10.1088/1464-4258/9/8/S06.
[51] J. W. Chan, *J. Biophoton.* **2013**, *6*, 36, https://doi.org/10.1002/jbio.201200143.
[52] M. Navas-Moreno, J. W. Chan, in 'Cellular Heterogeneity', Vol. 1745, Eds. N. S. Barteneva, I. A. Vorobjev, Springer New York, New York, NY, **2018**, pp. 219, https://doi.org/10.1007/978-1-4939-7680-5_13.
[53] D. Pontoni, J. Bolze, N. Dingenouts, T. Narayanan, M. Ballauff, *J. Phys. Chem. B* **2003**, *107*, 5123, https://doi.org/10.1021/jp0343640.
[54] A. Cao, *Anal. Lett.* **2003**, *36*, 3185, https://doi.org/10.1081/AL-120026567.
[55] M. Alexander, D. G. Dalgleish, *Food Biophys.* **2006**, *1*, 2, https://doi.org/10.1007/s11483-005-9000-1.
[56] J. Lim, S. P. Yeap, H. X. Che, S. C. Low, *Nanoscale Res. Lett.* **2013**, *8*, 381, https://doi.org/10.1186/1556-276X-8-381.
[57] R. Xu, *Particuology* **2015**, *18*, 11, https://doi.org/10.1016/j.partic.2014.05.002.
[58] P. M. Carvalho, M. R. Felício, N. C. Santos, S. Gonçalves, M. M. Domingues, *Front. Chem.* **2018**, *6*, 237, https://doi.org/10.3389/fchem.2018.00237.
[59] J. Stetefeld, S. A. McKenna, T. R. Patel, *Biophys. Rev.* **2016**, *8*, 409, https://doi.org/10.1007/s12551-016-0218-6.
[60] R. Pecora, Ed. , 'Dynamic light scattering: applications of photon correlation spectroscopy', Plenum Press, New York, N.Y., **1985**.
[61] O. Urquidi, N. Barbosa, J. Brazard, T. B. M. Adachi, *Rev. Sci. Instrum.* **2023**, *94*, 083101, https://doi.org/10.1063/5.0160156.
[62] O. Urquidi, J. Brazard, T. B. M. Adachi, Proc. SPIE **2023**, 12672, 1267209, https://doi.org/10.1117/12.2677534.
[63] P. D. Kaplan, V. Trappe, D. A. Weitz, *Appl. Opt.* **1999**, *38*, 4151, https://doi.org/10.1364/AO.38.004151.
[64] T. Hiroi, M. Shibayama, *Opt. Express* **2013**, *21*, 20260, https://doi.org/10.1364/OE.21.020260.
[65] T. Hiroi, S. Samitsu, K. Ishioka, *Sci. Technol. Adv. Mater.: Methods* **2021**, *1*, 134, https://doi.org/10.1080/27660400.2021.1957403.
[66] A. V. Malm, J. C. W. Corbett, *Sci. Rep.* **2019**, *9*, 13519, https://doi.org/10.1038/s41598-019-50077-4.
[67] T. A. Laurence, S. Fore, T. Huser, *Opt. Lett.* **2006**, *31*, 829, https://doi.org/10.1364/OL.31.000829.

License and Terms

The definitive version of this article is the electronic one that can be found at https://doi.org/10.2533/chimia.2024.50